Research Square

Preprints are preliminary reports that have not undergone peer review.
They should not be considered conclusive, used to inform clinical practice,
or referenced by the media as validated information.

COL6A2 as a key regulator of extracellular matrix remodeling and nucleus pulposus cell migration in intervertebral disc degeneration

Longquan Lin

467796153@qq.com

the 910th Hospital of PLA

Huimin Cai

the 910th Hospital of PLA

Peiji Chen

the 910th Hospital of PLA

Gangfeng Cai

Fujian Medical University Union Hospital

Rongzi Chen

the 910th Hospital of PLA

Da Li

the 910th Hospital of PLA

Kun Chen

the 910th Hospital of PLA

Ruijin You

the 910th Hospital of PLA

Article

Keywords: COL6A2, Intervertebral disc degeneration, Extracellular matrix remodeling, Bioinformatics, Biomarker

Posted Date: November 6th, 2026

DOI: https://doi.org/10.21203/rs.3.rs-11399270/v1

License: This work is licensed under a Creative Commons Attribution 4.0 International License.
Read Full License

Additional Declarations: No competing interests reported.

COL6A2 as a key regulator of extracellular matrix remodeling and nucleus pulposus cell migration in intervertebral disc degeneration

Longquan Lin[1,*], Huimin Cai[1], Peiji Chen[1,*], Gangfeng Cai[2], Rongzi Chen[1], Da Li[1], Kun Chen[1], Ruijin You[1,*]

[1] Department of Orthopaedics, the 910th Hospital of PLA, Quanzhou 362000, China

[2] Department of Neurosurgery, Fujian Medical University Union Hospital, Fuzhou 350000, China

Longquan Lin, Huimin Cai, Peiji Chen contributed equally to this work.

* Correspondence: Longquan Lin (467796153@qq.com); Peiji Chen (huaihuai28@163.com); Ruijin You (13959729666@163.com).

Abstract

Clinical consensus holds that intervertebral disc degeneration (IVDD) is the most important etiology of discogenic pain. The essence of IVDD is the disruption of extracellular matrix (ECM) homeostasis. COL6A2 is an ECM structural protein, but its role in IVDD is not understood. We analyzed two GEO datasets (GSE70362 and GSE124272) for differential gene expression. We intersected the results with ECM metabolism-related genes from PathCards and obtained 39 ECM-related genes. GO and KEGG enrichment, PPI network construction, and CytoHubba were used to identify hub genes. COL6A2 expression was measured by RT-qPCR in clinical NP tissues. The needle-puncture model in mice was constructed. COL6A2 was knocked down in NP cells with lentivirus-delivered shRNA. COL6A2 emerged as the predominant hub gene. COL6A2 was significantly upregulated in degenerated NP tissues. Knockdown of COL6A2 reduced ADAMTS8, Aggrecan, LAMC1, and ITGA9 expression, suppressed phosphorylation of PI3K, FAK, Akt, and ERK1/2, and impaired cell migration and proliferation. LY294002 treatment phenocopied these ECM defects, confirming that COL6A2 regulates ECM homeostasis via the PI3K-Akt signaling pathway. These findings demonstrate that COL6A2 functions as an upstream coordinator of ECM homeostasis, orchestrating ECM remodeling and NP cell migration, and that its dysregulation in IVDD may actively drive the degenerative cascade.

Keywords: COL6A2; Intervertebral disc degeneration; Extracellular matrix remodeling; Bioinformatics; Biomarker

Introduction

IVDD is a common degenerative disease and a main cause of discogenic pain and functional impairment worldwide, imposing a heavy burden on a large number of patients [1,2]. The pathophysiological process of IVDD is the progressive structural disruption of the intervertebral disc, including loss of matrix water, formation of fissures and tears, and collapse of the intervertebral disc space [3]. At the molecular level, IVDD involves genetic susceptibility, mechanical overload, inflammatory responses, etc., but the most crucial aspect is the complex interaction of metabolic disorders of the extracellular matrix (ECM) [4,5].

The ECM of intervertebral discs mainly consists of collagens, proteoglycans and glycoproteins. These molecules provide structural integrity and biomechanical function to the disc. The core pathogenic mechanism in IVDD is that ECM synthesis and degradation become imbalanced which leads to progressive matrix depletion [6]. Matrix metalloproteinases (MMPs) and members of a disintegrin and metalloproteinase with thrombospondin motifs (ADAMTS) family are the key enzymes that degrade the ECM during IVDD progression [7]. On the contrary, ECM components such as aggrecan and laminins are helpful in preserving disc architecture and ensuring cellular homeostasis of the intervertebral disc [8].

COL6A2 encodes the α-2 chain of type VI collagen, which is the main ECM component for forming microfibrillar lattices in various connective tissues [9]. In addition to its structural role, COL6A2 has been shown to participate in cell adhesion, signal transduction pathways, and migration [10,11]. Recent studies have shown that COL6A2 is abnormally expressed under various pathological conditions, including gliomas, clear cell renal cell carcinoma, and lung adenocarcinoma. COL6A2 regulates tumor progression through integrin-mediated signaling pathways (Wnt/β-catenin and PI3K-Akt) [12,13,14]. It is worth noting that a recent bioinformatics study identified COL6A2 as a potential diagnostic marker for IVDD based on single-cell and bulk RNA-seq analyses [15]. Very recently, soluble type VI collagen has been shown to promote human nucleus pulposus (NP) cell proliferation and IGF-1 expression through ERK signaling, underscoring the signaling capacity of type VI collagen in the disc niche [16]. However, the main role of COL6A2 in IVDD and its control of NP cell and ECM metabolism behavior remain unclear.

In our study, we explore the abundance and functional significance of COL6A2 in IVDD. We used the GEO datasets to perform differential expression analysis. We validated COL6A2 expression in clinical NP tissue, and systematically examined the impact of COL6A2 silencing on ECM-related genes expression and NP cell migration. At the same time, we validated the effects of COL6A2 knockdown on the FAK/PI3K-Akt/ERK phosphorylation cascade at the level of signalling pathway proteins, and preliminarily established the mediating role of the PI3K-Akt pathway in this process through pharmacological intervention with a PI3K inhibitor. Our results provide a new understanding of the molecular mechanisms driving IVDD and highlight the importance of COL6A2 as an interventional target.

Methods

Bioinformatics analysis

Download two datasets related to IVDD (GSE70362 and GSE124272) from the GEO database. The GSE70362 dataset comprises 48 samples exhibiting varying degrees of disc degeneration.

Based on reference [15], Pfirrmann grades I–III were defined as the mild group (IVDD_M) and grades IV–V as the severe group (IVDD_S) for the purposes of comparative analysis. The GSE124272 dataset comprises 8 samples of disc herniation and 8 healthy controls; of note, GSE70362 contains only degenerated samples of different severities and was therefore used for severity-based comparisons, whereas GSE124272 was used for the disease-versus-health comparison. Differential expression analysis was conducted with the R package Limma, screening for genes with a cutoff of $|logFC| > 0.55$ and $P < 0.05$.

Differential expression analysis

After batch correction of the count matrix, we used the Limma R package (v3.56.2) to analyse DEGs between IVDD and control samples. The cutoffs were $|logFC| > 0.6$ and $P < 0.05$. Volcanic representations were drawn to show the distribution of DEGs.

Identification of ECM metabolism-related genes

We searched the PathCards website (https://pathcards.genecards.org/) with the keyword "Extracellular matrix" to obtain ECM metabolism-related genes. The DEGs from the two datasets were then intersected with this gene set to obtain the overlapping genes.

Functional enrichment analysis

GO and KEGG enrichment analyses were conducted using the ClusterProfiler package (v4.13.4) within the R environment. GO and KEGG enrichment pathways for which both nominal P-value and adjusted P-value were < 0.05 were treated as reaching statistical significance [17-20].

PPI network construction

Submit the above set of overlapping genes to the String website (https://string-db.org/) for PPI analysis. Analyse the interactions between proteins to identify direct relationships between them. KEGG results for the relevant genes were extracted, and the interactions between genes and pathways were visualised using Cytoscape (v3.9.0). The Cytohubba plugin was used to identify hub genes, and the gene ranking first in the topological analysis was identified as the core gene. The resulting network diagram depicts the COL6A2-extracellular matrix metabolism-related gene pathway [21].

Clinical tissue samples and RT-qPCR validation

Human NP specimens were procured from 20 patients who underwent spinal surgery. Ten patients with lumbar trauma received discectomy (control group), and 10 patients with Pfirrmann grade III-IV IVDD received lumbar fusion (degeneration group). Total RNA was extracted using TRIzol reagent. RT-qPCR was conducted with the SYBR Green-based master mix on the StepOnePlus PCR system. Using beta-actin as an internal control, mRNA levels were quantified via the comparative Ct ($2^{(-\Delta\Delta Ct)}$) method. Ratified by the Ethics Committee (Approval No. [2024]94), the study adhered to the Declaration of Helsinki, and all participants completed an informed consent document.

Establishment of the mouse IVDD model

Eleven 6-week-old C57BL/6 mice were randomly allocated to the control group (Group I1, n = 3) and the model group (Group J1, n = 8). After intraperitoneal anesthesia with 1.25%

tribromoethanol (0.2 mL/10 g body weight), the L4–L5 disc was punctured with an 18G needle to a depth of approximately 2–3 mm, and the needle was then rotated to disrupt the internal disc structure. Antibiotics were administered post-operatively to prevent infection, for a period of 3–5 days. Four weeks later, the animals were euthanised by cervical dislocation, and NP tissue was collected for primary cell culture (Figure 1). All procedures involving animals were approved by the Animal Ethics Committee (Approval No. [2025]19).

Histological evaluation of IVDD

After the establishment of the IVDD model, lumbar vertebral tissues were harvested from the euthanised mice. Trimmed the specimens and fixed them in 4% formalin for one day, then decalcified them in 10% EDTA solution. The decalcified specimens underwent gradient ethanol dehydration, were paraffin-embedded, and cut into 4-μm-thick sections. The remaining specimens were stored in a freezer at –80°C for primary cell culture [22]. HE staining (H9627-25G, Sigma) was used to examine disc histopathology. Toluidine blue staining (71041284, Wokai) and Safranin-fast green staining (G1371, Solarbio) were used to analyse cartilage regeneration. We compared the morphology of the control and model groups to confirm that the model was established successfully.

Mouse primary NP cell isolation and culture

Isolate primary NP cells by digested NP tissue with 0.2% type II collagenase and 0.1% trypsin at 37°C for 3 hours. The cells were maintained in complete medium supplemented with 10% FBS under standard conditions (37°C, 5% CO_2). The cells were passaged when their confluence reached over 85%, and use them from passage 2-3 for subsequent experiments [23].

Lentivirus-mediated shRNA knockdown

To build a stable COL6A2-knockdown cell model, we used lentivirus-mediated RNA interference. shRNA sequences against COL6A2 (shRNA-KD) and non-targeting control sequences (shRNA-NC) were cloned into lentiviral vectors. The recombinant plasmids were purchased from Wuhan MiaoLing Biotechnology Co. After packaging the lentivirus, transfect NP cells in accordance with the instructions. COL6A2 mRNA expression levels were checked by RT-qPCR 72 hours after infection, and the most effective shRNA construct was used in the functional assays [24].

RNA isolation and RT-qPCR

Total RNA was isolated using the TRIzol reagent (Invitrogen, USA). cDNA was reverse-transcribed using the EntiLink reverse transcription kit (ELK Biotechnology, EQ003, Wuhan, China). RT-qPCR was conducted using the EnTurbo™ SYBR Green PCR Master Mix (ELK Biotechnology, EQ001, Wuhan, China) on the StepOne™ Real-Time PCR System (Life Technologies, USA). The primer pairs are listed in Table 1. The target genes were COL6A2, LAMC1, ITGA9, ADAMTS-8, Aggrecan and beta-actin (internal reference). mRNA levels were quantified via the comparative Ct ($2^{(-\Delta\Delta Ct)}$) method.

Western blot analysis

We extracted total proteins from NP cells by lysing them in RIPA buffer supplemented with phosphatase and protease inhibitors (AS1004, ASPEN). The total protein content was determined

using the BCA Protein Concentration Assay Kit (AS1086, ASPEN). Protein samples (40 μg per lane) were resolved by SDS-PAGE (stacking gel at 80 V, resolving gel at 120 V) and then electroblotted onto a 0.45-μm PVDF membrane (Millipore, IPVH00010) at a constant current of 300 mA. The membranes were blocked with 5% non-fat dry milk for 1 h at room temperature, followed by overnight incubation at 4°C with primary antibodies against ADAMTS-8, Aggrecan, p-PI3K, p-FAK, t-FAK, p-Akt, t-Akt, p-ERK1/2, t-ERK1/2, or β-actin. After washing with TBST, the membranes were probed with HRP-linked secondary antibodies for 30 min at room temperature. Used the enhanced chemiluminescence (ECL) substrate (AS1059, ASPEN) to visualise protein bands, and expose and develop the film in a darkroom. AlphaEaseFC software was used to quantify the band densities, and the target protein levels were normalized to β-actin.

Wound healing assay

NP cells were seeded in 6-well culture dishes and grown to 90% confluency. We used a sterile 200-μL disposable pipette tip to create uniform scratch wounds in each well. We washed the cells with PBS to get rid of cell debris, then moved them to serum-free DMEM/F12 medium. Photos of the scratch healing process were taken with a standard inverted microscope at 0, 12, and 24 h. The formula for calculating the wound closure rate was: (width at 0 hours – width at T hours) / width at 0 hours × 100%. Each experiment was done three times on its own, and we used three wells per repeat.

CCK-8 cell proliferation assay

NP cells from each group were seeded into a 96-well plate at 5×10^3 cells/well (100 μl/well), using 6 wells per repeat. At the same time, set up blank control wells (containing only culture medium, with no cells). Incubated the cells in a 37°C and 5% CO_2 incubator for 48 hours. Ten microliters of CCK-8 reagent (Beyotime, C0038) was added to each well, then the plates were left at 37°C in the dark for 2 h. The optical density (OD) of each well was read at 450 nm using a microplate reader. Relative cell proliferation rate = [(experimental OD − blank OD) / (control OD − blank OD)] × 100%.

Pharmacological intervention study with the PI3K inhibitor LY294002

To validate the mediating role of the PI3K-Akt signalling pathway in the regulation of ECM homeostasis by COL6A2, we administered the PI3K-specific inhibitor LY294002 (MCE, HY-10108) to normal (non-knockdown) NP cells. An initial CCK-8 assay was performed to determine the optimal concentration. Normal NP cells were treated with either a solvent control (DMSO, final concentration ≤0.1%) or LY294002 at 10, 15, and 20 μM for 48 h, followed by assessment of cell viability. The highest concentration that did not significantly affect cell viability was selected for subsequent experiments. In the formal experiment, normal NP cells were treated with DMSO (control group) or LY294002 for 48 h. Total protein was extracted, and Western blot analysis was conducted to evaluate the protein levels of p-Akt, t-Akt, ADAMTS-8, and Aggrecan.

Statistical analysis

Data are expressed as mean ± SD from at least three independent experiments. All statistical tests were performed using SPSS version 25.0. Differences between three or more groups were analysed by one-way ANOVA followed by the LSD test for pairwise analyses. A P-value < 0.05

was considered statistically significant, and significance levels were indicated by asterisks (*P < 0.05, **P < 0.01, ***P < 0.001).

Results

Bioinformatics analysis identifies COL6A2 as a core ECM regulatory gene in IVDD

In the GSE70362 dataset (n = 48), differential expression analysis with cutoffs of |logFC| > 0.55 and P < 0.05 identified 254 DEGs, including 93 upregulated and 161 downregulated genes. COL6A2 expression was downregulated in the severe degeneration group (IVDD_S) compared with the mild group (IVDD_M). This suggests that COL6A2 may be compensatorily upregulated in early degeneration. The volcano plot is shown in Figure 2a. In the GSE124272 dataset, we found 1,563 DEGs (589 upregulated and 974 downregulated). COL6A2 was significantly upregulated in disc herniation samples compared with healthy controls (logFC = 1.32, P < 0.01; Figure 2b), consistent with its compensatory upregulation in early degeneration.

A search of PathCards with the keyword "Extracellular matrix" returned two SuperPaths: extracellular matrix organization and articular cartilage extracellular matrix. The first SuperPath contained two pathways (ECM organization and ECM degradation) with 300 genes in total. We intersected the DEGs of the two datasets with these 300 ECM-related genes. Extracted 18 overlapping genes between GSE70362 and Extracellular genes, and 22 overlapping genes between GSE12427 and Extracellular genes; combining them results in a total of 39 genes. Creating a Venn diagram (Figure 2c). These genes include key ECM molecules such as COL6A2, ITGA9, LAMC1, Aggrecan, MMP1 and MMP2.

GO analysis showed strong enrichment in ECM organization ($P = 2.99 \times 10^{-23}$), ECM disassembly ($P = 1.02 \times 10^{-10}$), and collagen metabolic process ($P = 3.02 \times 10^{-7}$). KEGG analysis found 12 enriched pathways, including ECM-receptor interaction ($P = 4.77 \times 10^{-9}$), PI3K-Akt signaling ($P = 7.53 \times 10^{-5}$), and focal adhesion ($P = 1.67 \times 10^{-6}$) (Figure 2d).

These pathways are intimately involved in ECM metabolism and the regulation of cellular behaviour. PPI network analysis revealed 36 direct interactions amongst 39 ECM-associated proteins. KEGG results were extracted and the interactions between genes and pathways were visualised in Cytoscape (3.9.0) software (Figure 2e). The results show that COL6A2 ranked first with the highest score (4,004,950), followed by COL5A2 (4,004,664) and COL12A1 (4,004,522). This demonstrates that COL6A2 occupies a central hub position within the ECM regulatory network. COL6A2 directly regulates key ECM genes such as LAMC1 and ITGA9 via the ECM-receptor interaction pathway, indicating that COL6A2 contributes to the pathological process of IVDD by influencing the expression of these genes.

COL6A2 is upregulated in degenerated NP tissues

In the GSE124272 dataset (8 disc herniation vs. 8 healthy controls), COL6A2 was significantly up-regulated in degenerated intervertebral disc tissue compared with healthy controls (logFC = 1.32, P < 0.01). In the GSE70362 severity-based comparison, COL6A2 expression was higher in the mild (IVDD_M) than in the severe (IVDD_S) group, indicating that COL6A2 is preferentially elevated at early stages of degeneration. RT-qPCR on clinical NP tissue samples confirmed that COL6A2 mRNA expression was markedly elevated in the IVDD cohort relative to the control

cohort, aligning with the bioinformatics analysis. These data have been validated and published in previous studies [25].

Histological validation of the mouse IVDD model

We performed HE, Safranin O/fast green, and toluidine blue staining on mouse lumbar vertebral tissues from the control (Group I1, n = 3) and model (Group J1, n = 8) groups to ensure the model's fidelity, with a focus on architectural differences in the intervertebral disc. HE staining revealed that the control group exhibited intact tissue microarchitecture within the discs, with the NP exhibiting normal histological features: the NP was rich in cells arranged in an orderly manner, and the extracellular matrix was uniform. In the model cohort, the intervertebral disc's histoarchitectural integrity was severely compromised, characterized by marked NP cell loss, extensive extracellular matrix breakdown, and disruption of the annulus fibrosus (AF) lamellar architecture, collectively recapitulating hallmark features of disc degeneration. Histochemical interrogation using Safranin O and Fast Green documented intense orthochromatic red signal within the nucleus pulposus (NP) of control specimens, reflecting robust proteoglycan retention in the native disc matrix; red staining in the NP region of the model group was significantly reduced, suggesting a substantial loss of proteoglycan. Toluidine blue histochemistry documented intense metachromatic purple-red labeling within the control nucleus pulposus (NP) compartment, reflecting robust retention of proteoglycans and sulfated glycosaminoglycans (sGAGs); by contrast, in the established IVDD model cohort, metachromatic signal was markedly attenuated with only faint orthochromatic blue residual staining, attesting to profound depletion of sulfated glycosaminoglycans (sGAGs) and resident proteoglycans. Collectively, the histopathological evidence from the aforementioned staining panels validates the successful induction of intervertebral disc degeneration in mice via needle puncture, with the model faithfully recapitulating core phenotypic hallmarks of clinical IVDD; intervertebral disc parenchyma in the IVDD-modeled cohort exhibited typical degenerative changes, providing a reliable animal model basis for subsequent studies on COL6A2 function (Figure 3).

Efficient COL6A2 knockdown in NP cells

To further delineate the functional relevance of COL6A2 in NP cell pathophysiology, we transduced primary mouse NP cells with lentiviral vectors encoding COL6A2-targeting shRNAs. Three shRNA sequences were used (C1: COL6A2 shRNA-1; D1: COL6A2 shRNA-2; E1: COL6A2 shRNA-3). RT-qPCR validation revealed robust, consistent COL6A2 knockdown across the triplicate COL6A2 shRNA-KD samples, with transcript levels substantially lower than those in control (A1) and shRNA-NC (B1) NP cells stably expressing the scramble construct. The most effective construct (COL6A2 shRNA-1) achieved a knockdown efficiency of approximately 73.6%. COL6A2 mRNA levels showed no significant intergroup variance between control (A1) and shRNA-NC (B1) NP cells, validating that the robust knockdown observed across the triplicate COL6A2 shRNA-KD samples reflects genuine sequence-specific silencing (Figure 4a). COL6A2 shRNA-1 was selected for the next stage of the experiments.

COL6A2 knockdown suppresses ECM-related gene expression

We further used RT-qPCR to investigate the effects of COL6A2 knockdown on ECM-related genes. COL6A2 knockdown reduced ADAMTS8 mRNA by about 53.3% ($P < 0.0001$) and

Aggrecan mRNA by about 42.5% ($P = 0.0006$) (Figure 4b-c). Additional RT-qPCR showed that LAMC1 mRNA fell by about 44.7% ($P = 0.0011$) and ITGA9 mRNA by about 58.3% ($P < 0.0001$) (Figure 4d-e). No statistically meaningful variance was detected in the expression of all four assayed genes between control and shRNA-NC NP cells, validating that the phenotypic shifts in the triplicate COL6A2 shRNA-KD group are exclusively driven by COL6A2 depletion, not nonspecific shRNA effects. Collectively, the above loss-of-function evidence from triplicate COL6A2 shRNA knockdown assays demonstrates that COL6A2 serves as a pivotal upstream transcriptional modulator governing the steady-state transcript levels of multiple ECM-associated genes in primary mouse NP cells.

COL6A2 knockdown reduces ADAMTS-8 and Aggrecan protein levels

To confirm the effect of COL6A2 knockdown at the protein level, we selected two genes of key relevance to the ECM (ADAMTS-8 and Aggrecan) and performed Western blot analysis (Figure 5a). ADAMTS-8 protein (normalized to beta-actin) fell from 0.51 ± 0.10 in the control group to 0.16 ± 0.08 in the COL6A2 shRNA-1 group ($P = 0.0037$), a drop of about 68.6%. Aggrecan protein fell from 0.82 ± 0.12 to 0.17 ± 0.09 ($P = 0.0003$), a drop of about 79.3%. No divergence was detected between the control group and the shRNA-NC group, confirming the specific effect of COL6A2 knockdown on ECM protein expression (Figure 5b-c).

COL6A2 silencing impairs NP cell migration

Wound healing assays probed COL6A2's effect on NP cell motility (Figure 6a). COL6A2 knockdown significantly impaired NP cell migration at both time points. At 12 hours, the wound closure rate was $29.1\% \pm 0.9\%$ in the control group, $31.5\% \pm 1.5\%$ in the shRNA-NC group, and $19.5\% \pm 1.2\%$ in the COL6A2 shRNA-1 group ($P < 0.001$ vs. control). At 24 hours, the difference was even more pronounced: the healing rates in the control group and the shRNA-NC group were $77.7\% \pm 0.7\%$ and $77.3\% \pm 0.5\%$ respectively, whilst the COL6A2 shRNA-1 group achieved a wound closure rate of only $48.7\% \pm 1.2\%$ ($P < 0.0001$ vs. control) (Figure 6b). Data show COL6A2 is essential for NP cell locomotion, and its silencing significantly impairs cell motility.

COL6A2 knockdown inhibits NP cell proliferation

To assess COL6A2's regulatory impact on NP cell proliferative capacity, we performed a CCK-8 assay. CCK-8 data revealed COL6A2 KD markedly reduced NP cell proliferative capacity. The relative proliferation rate was $100.0\% \pm 7.0\%$ in the control group (F1), $96.9\% \pm 4.9\%$ in the shRNA-NC group (G1, $P = 0.387$ vs. control), and $54.3\% \pm 8.4\%$ in the COL6A2 shRNA-1 group (H1). A reduction of approximately 45.7% relative to the control group ($P < 0.0001$) (Figure 6c). This indicates that COL6A2 silencing significantly inhibits the proliferative capacity of NP cells. No significant divergence was detected between the control group and the shRNA-NC groups, confirming that the observed inhibition of proliferation was specific to COL6A2 knockdown. The reduction in cell proliferative capacity may be associated with impaired COL6A2-regulated ECM-integrin signalling pathways, further supporting the key regulatory role of COL6A2 in maintaining NP cell function.

COL6A2 silencing suppresses FAK/PI3K-Akt/ERK pathway phosphorylation

To assess COL6A2's role in signaling, we compared phosphorylation of FAK/PI3K-Akt/ERK nodes between shRNA-NC and COL6A2 shRNA-1 NP cells (Figure 7a). COL6A2 knockdown markedly reduced all phosphorylated proteins: p-PI3K (0.40±0.09 to 0.07±0.02, P=0.003, ~82% decrease), p-FAK (0.31±0.06 to 0.08±0.03, P=0.004, ~75% decrease), p-Akt (0.34±0.12 to 0.12±0.06, P=0.044, ~65% decrease), and p-ERK1/2 (1.19±0.42 to 0.34±0.17, P=0.031, ~72% decrease). By contrast, total protein levels remained unchanged: t-PI3K (0.51±0.07 vs. 0.51±0.07, P=0.975), t-FAK (0.85±0.10 vs. 0.83±0.08, P=0.793), t-Akt (0.84±0.18 vs. 0.81±0.19, P=0.864), and t-ERK1/2 (1.97±0.55 vs. 1.95±0.48, P=0.963) (Figure 7b). These data indicate that COL6A2 silencing selectively inhibits FAK-PI3K-Akt and ERK phosphorylation without affecting total protein expression, placing COL6A2 upstream of these cascades.

Pharmacological PI3K-Akt blockade phenocopies the ECM defects caused by COL6A2 silencing

To determine whether PI3K-Akt inhibition mirrors the effects of COL6A2 knockdown, normal NP cells were exposed to the PI3K inhibitor LY294002. CCK-8 viability assays identified 15 μM as the highest non-cytotoxic concentration (10 and 15 μM: 101.8%±4.2% and 97.5%±3.7% vs. 100.0%±4.0% control, P>0.05; 20 μM: 88.4%±3.2%, P<0.05) (Figure 8a). Treatment with 15 μM LY294002 strongly suppressed p-Akt (0.46±0.08 to 0.10±0.03, P=0.002, ~78% decrease) without altering t-Akt levels (0.78±0.17 vs. 0.78±0.17, P=0.992) (Figure 8b-c). Similarly, ADAMTS-8 and Aggrecan protein levels were markedly reduced, dropping from 0.52±0.13 to 0.11±0.03 (P=0.006, ~79% decrease) and from 0.56±0.16 to 0.18±0.06 (P=0.020, ~67% decrease), respectively. These alterations closely paralleled the ECM phenotype observed after COL6A2 silencing, demonstrating that targeted PI3K-Akt inhibition is sufficient to recapitulate COL6A2 loss and that sustained PI3K-Akt signaling is essential for preserving ECM protein expression in NP cells.

Discussion

Our work converges computational screening with cellular assays to delineate how COL6A2 orchestrates the pathogenesis of IVDD. Three lines of evidence support this conclusion. (1) Through differential expression analysis of two datasets and the construction of a PPI network, it has been demonstrated that COL6A2 is a core hub gene in the ECM regulatory network. It forms a close-knit network of protein interactions with COL5A2, COL12A1, LAMC1 and ITGA9. (2) Loss of COL6A2 function dampens ADAMTS-8 output and aggrecan deposition at transcript and protein scales, establishing COL6A2 as a proximal modulator that sits upstream of the core ECM homeostatic program in intervertebral disc cells. (3) Silencing of COL6A2 significantly impairs the migration and proliferation of NP cells, suggesting that it regulates NP cell function via integrin-mediated signalling pathways. (4) COL6A2 silencing markedly suppresses FAK/PI3K-Akt/ERK pathway phosphorylation and activation, whereas the PI3K inhibitor LY294002 mirrors the downregulation of ADAMTS-8 and Aggrecan proteins triggered by COL6A2 loss in normal NP cells, thus establishing the PI3K-Akt cascade as a key downstream effector of COL6A2 in governing ECM homeostasis. Collectively, our data transcend the conventional view of COL6A2 as merely a structural determinant in IVDD, positioning type VI collagen as a critical signaling effector within the disc niche that actively orchestrates the extracellular microenvironment.

The special position of type VI collagen in intervertebral discs stems from its dual biological functions. Unlike Type I and Type II collagens which form fibres, Type VI collagen assembles into beaded filaments within the ECM. These can form a unique network of microfibres that is widely distributed within the pericellular matrix (PCM) of the NP cells [9,37]. The C5 domain of the α3 chain of type VI collagen can be cleaved extracellularly by proteases such as BMP-1 and proprotein convertases, forming a bioactive fragment known as endotrophin (ETP) [26,27]. Building on emerging evidence, Kim et al. [29] utilised an ETP-specific knockout mouse model to selectively delete endotrophin rather than the entire COL6A3 molecule, thereby significantly reducing the progression of fibrosis after renal ischaemia-reperfusion injury. COL6A2-derived endotrophin orchestrates both the priming and chronic perpetuation of fibrotic remodeling and progressive nucleus pulposus matrix deterioration within the hypoxic disc niche. This provides an important explanation for the widespread downregulation of ECM-related genes after COL6A2 knockdown.

The most noteworthy finding and warranting further discussion of this study is that COL6A2 silencing simultaneously reduced the expression of both ADAMTS-8 (an ECM-degrading enzyme) and Aggrecan (a structural component of the ECM). At first glance this seems paradoxical, but it actually reveals the role of COL6A2 as a master regulator of ECM homeostasis. ADAMTS-8 belongs to the ADAMTS metalloproteinase family and has aggrecanase activity. It is responsible for aggrecan degradation in cartilage and disc tissues [7,29]. In our study, however, both ADAMTS-8 and Aggrecan decreased after COL6A2 knockdown. This indicates that COL6A2 does not control single degradative enzymes or structural genes. Instead, it coordinates the transcriptional program of ECM metabolism at a higher level. A plausible mechanism is that COL6A2 regulates the expression of multiple ECM genes, including ADAMTS8 and ACAN, through integrin-mediated outside-in signaling [31]. Type VI collagen binds directly to integrins alpha-1 beta-1 and alpha-2 beta-1 [9,27]. The downstream FAK/PI3K/Akt and MAPK pathways are major intracellular routes that control ECM gene expression. COL6A2 dysregulation may affect both ECM-degrading enzymes and structural proteins through the integrin/FAK/PI3K-Akt axis. From a pathophysiological perspective, the upregulation of COL6A2 in the early stages of IVDD may represent a compensatory protective response. However, as the degenerative process progresses, the sustained overexpression of COL6A2, accompanied by upregulation of ADAMTS-8, actually exacerbates ECM degradation and create a vicious cycle. This dual nature helps to explain the different biological effects that COL6A2 may exert at different stages of IVDD.

Our signaling assays provide direct protein-level evidence for this model. COL6A2 silencing caused a coordinated drop in p-FAK, p-PI3K, p-Akt, and p-ERK without changing total protein levels, consistent with an upstream–downstream hierarchy: reduced COL6A2 weakens VI collagen–β1 integrin binding, dampening FAK autophosphorylation at focal adhesions and subsequent PI3K-Akt/ERK signaling [9,30,32]. Pharmacological phenocopy further validated this link: in normal NP cells, LY294002-mediated PI3K inhibition alone downregulated ADAMTS-8 and Aggrecan, matching the knockdown phenotype. This indicates that basal PI3K-Akt activity is required to maintain ECM protein expression, and that COL6A2 loss disrupts ECM at least partly through this cascade.

Parallel wound healing and CCK-8 proliferation profiling further corroborated that COL6A2 depletion markedly curtailed wound closure rate and cell proliferation of mouse primary NP cells, aligning with its regulatory role in disc ECM homeostasis. In both the physiological matrix turnover of healthy nucleus pulposus and the pathological fibrotic remodeling of degenerated discs, the migratory capacity of NP cells underpins endogenous tissue repair—a phenotype our wound healing assays show is attenuated by COL6A2 silencing [28,32]. The migration of NP cell is an active process that is precisely regulated by the integrin family. Integrin receptors recognise specific ligand sequences in the ECM (such as the RGD and GFOGER sequences) and drive cytoskeletal reorganisation and cell migration through phosphorylation cascade involving focal adhesion kinase (FAK) and paxillin [32,33]. In a normal intervertebral disc, the microfibril network formed by type VI collagen provides an adhesive matrix and migration pathways for NP cells. We observed a reduction of approximately 45.7% in cell proliferation following COL6A2 knockdown in NP cells. These findings demonstrate COL6A2 serves a key regulatory role in the proliferative activity of NP cells. KEGG pathway analysis revealed that PI3K-Akt and TGF-beta were the most significantly enriched signalling pathways and the crosstalk between them may play a central role in COL6A2-mediated modulation of migration. Activation of the PI3K-Akt pathway promotes cytoskeletal reorganisation and cell motility, whilst the TGF-beta pathway is the primary driver of ECM synthesis and fibrosis [33,34]. Moderate mechanical loading maintains the NP cell phenotype and matrix synthesis via the integrin/FAK signalling pathway. Whereas excessive or abnormal loading triggers inflammation and matrix degradation via the same pathway [35,36]. As a major component of the ECM, type VI collagen acts as the first checkpoint through which mechanical signals are transmitted into NP cells.

This study has certain shortcomings. To begin with, the clinical validation cohort was relatively small, and there has been no systematic assessment of the dynamic changes in COL6A2 expression at different stages of degeneration. Larger-scale with multi-time-point cohort are required to establish a quantitative relationship between COL6A2 abundance and the severity of IVDD. Secondly, although our in vitro experiments have demonstrated the functional importance of COL6A2 in NP cells, its biological effects within the complex in vivo microenvironment still need to be validated with conditional Col6a2 knockout mice or an intradiscal injection strategy. Thirdly, type VI collagen, to which COL6A2 belongs, is a heterotrimer formed by the assembly of three chains—alpha1(VI), alpha2(VI) and alpha3(VI). It remains unclear from this study whether COL6A2 knockdown affects the expression of other alpha chains or the overall assembly and secretion of type VI collagen.

In summary, by integrating computational bioinformatic profiling, primary clinical specimen validation and cell-based functional assays, this study systematically demonstrates the central mechanistic role of COL6A2 in IVDD pathogenesis and reveals its new role as a major regulator of ECM homeostasis. Our research confirms the central role of COL6A2 in regulating ECM remodelling and cell migration in the NP cell, and also elucidates the biological function of type VI collagen in IVDD from the three-dimensional perspective of ‘structural ECM components, signalling peptides, mechanical transduction’. These findings lay an important groundwork for advancing IVDD biomarkers and therapeutic approaches based on COL6A2 and its downstream signalling pathways.

Data availability

Publicly available datasets were analysed in this study. These data can be found here: Gene Expression Omnibus (GEO), GSE70362 (https://www.ncbi.nlm.nih.gov/geo/query/acc.cgi?acc=GSE70362) and GSE124272 (https://www.ncbi.nlm.nih.gov/geo/query/acc.cgi?acc=GSE124272). The original data presented in the study are included in the article or supplementary information files; further inquiries can be directed to the corresponding authors.The Supplementary Material for this article can be found online at 10.6084/m9.figshare.34711437.

References

1. Hammoor, B. T., Lai, C. S., Xiong, G. X. et al. Intervertebral disc degeneration. Nat. Rev. Dis. Primers 12, 5 (2026).

2. Oichi, T., Taniguchi, Y., Oshima, Y. et al. Pathomechanism of intervertebral disc degeneration. JOR Spine 3, e1076 (2020).

3. Xin, J., Wang, Y., Zheng, Z. et al. Treatment of intervertebral disc degeneration. Orthop. Surg. 14, 1271–1280 (2022).

4. Koroth, J., Buko, E. O., Abbott, R. et al. Macrophages and intervertebral disc degeneration. Int. J. Mol. Sci. 24, 1367 (2023).

5. Kirnaz, S., Capadona, C., Wong, T. et al. Fundamentals of intervertebral disc degeneration. World Neurosurg. 157, 264–273 (2022).

6. Vergroesen, P. P., Kingma, I., Emanuel, K. S. et al. Mechanics and biology in intervertebral disc degeneration: a vicious circle. Osteoarthr. Cartil. 23, 1057–1070 (2015).

7. Wang, W. J., Yu, X. H., Wang, C. et al. MMPs and ADAMTSs in intervertebral disc degeneration. Clin. Chim. Acta 448, 238–246 (2015).

8. Sivan, S. S., Wachtel, E. & Roughley, P. J. Structure, function, aging and turnover of aggrecan in the intervertebral disc. Biochim. Biophys. Acta 1840, 3181–3189 (2014).

9. Cescon, M., Gattazzo, F., Chen, P. et al. Collagen VI at a glance. J. Cell Sci. 128, 3525–3531 (2015).

10. Zhu, J., Lin, Q., Zheng, H. et al. The pro-invasive factor COL6A2 serves as a novel prognostic marker of glioma. Front. Oncol. 12, 897042 (2022).

11. Hong, X., Zhang, J., Zou, J. et al. Role of COL6A2 in malignant progression and temozolomide resistance of glioma. Cell. Signal. 102, 110560 (2023).

12. Yang, Y., Fan, R., Zhang, B. et al. COL6A2 in clear cell renal cell carcinoma: a multifaceted driver of tumor progression, immune evasion, and drug sensitivity. J. Transl. Med. 23, 875 (2025).

13. Ji, X., Yun, Y., Zhu, Z. et al. COL6A2 drives clear cell renal cell carcinoma progression via integrin-dependent modulation of Wnt/beta-catenin signaling. J. Cancer 16, 4426–4439 (2025).

14. Kong, F., Lu, Z., Xiong, Y. et al. A novel cancer-associated fibroblasts risk score model predict survival and immunotherapy in lung adenocarcinoma. Mol. Genet. Genomics 299, 70 (2024).

15. Song, H. M., Li, Z. W., Huang, Q. et al. A diagnostic signature for intervertebral disc degeneration using TNFAIP6 and COL6A2 based on single-cell RNA-seq and bulk RNA-seq analyses. Ann. Med. 57, 2443568 (2025).

16. Dalton, J., Divi, S. N., Eichbaum, Y. K. et al. The biological response of human nucleus pulposus cells to soluble collagen VI. Cells 15, 1339 (2026).

17. Wu, T., Hu, E., Xu, S. et al. clusterProfiler 4.0: A universal enrichment tool for interpreting omics data. Innovation 2, 100141 (2021).

18. Kanehisa, M., Furumichi, M., Sato, Y. et al. KEGG: biological systems database as a model of the real world. Nucleic Acids Res. 53, D672–D677 (2025).

19. Kanehisa, M. Toward understanding the origin and evolution of cellular organisms. Protein Sci. 28, 1947–1951 (2019).

20. Kanehisa, M. & Goto, S. KEGG: kyoto encyclopedia of genes and genomes. Nucleic Acids Res. 28, 27–30 (2000).

21. Ling, Z., Liu, Y., Wang, Z. et al. Single-cell RNA-seq analysis reveals macrophage involved in the progression of human intervertebral disc degeneration. Front. Cell Dev. Biol. 9, 833420 (2021).

22. Li, W., Ding, Z., Zhang, H. et al. The roles of blood lipid-metabolism genes in immune infiltration could promote the development of IDD. Front. Cell Dev. Biol. 10, 844395 (2022).

23. Han, P., Ivanovski, S., Crawford, R. et al. Activation of the canonical Wnt signaling pathway induces cementum regeneration. J. Bone Miner. Res. 30, 1160–1174 (2015).

24. Chen, J., Xia, Y., Peng, Y. et al. Analysis of the association between KIN17 expression and the clinical features/prognosis of epithelial ovarian cancer, and the effects of KIN17 in SKOV3 cells. Oncol. Lett. 21, 475 (2021).

25. Lin, L., Li, D., Cai, G. et al. Exploring the molecular mechanisms underlying intervertebral disc degeneration by analysing multiple datasets. Sci. Rep. 15, 14748 (2025).

26. Heumüller, S. E., Talantikite, M., Napoli, M. et al. C-terminal proteolysis of the collagen VI α3 chain by BMP-1 and proprotein convertase(s) releases endotrophin in fragments of different sizes. J. Biol. Chem. 294, 13769–13780 (2019).

27. Park, J. & Scherer, P. E. Adipocyte-derived endotrophin promotes malignant tumor progression. J. Clin. Invest. 122, 4243–4256 (2012).

28. Henriksen, K., Genovese, F., Reese-Petersen, A. et al. Endotrophin, a key marker and driver for fibroinflammatory disease. Endocr. Rev. 45, 361–378 (2024).

29. Kim, D. S., Funcke, J. B., Chen, S. et al. ETP-specific-knockout mice reveal endotrophin as a key regulator of kidney fibrosis in ischemia-reperfusion injury models. Exp. Mol. Med. 57, 2475–2486 (2025).

30. Wang, X., Tan, J., Sun, J. et al. Transcriptomics study to determine the molecular mechanism by which sIL-13Rα2-Fc inhibits caudal intervertebral disc degeneration in rats. Biomed. Res. Int. 2020, 7645989 (2020).

31. Tapial Martínez, P., López Navajas, P. & Lietha, D. FAK structure and regulation by membrane interactions and force in focal adhesions. Biomolecules 10, 179 (2020).

32. Humphries, J. D., Byron, A. & Humphries, M. J. Integrin ligands at a glance. J. Cell Sci. 119, 3901–3903 (2006).

33. Mitra, S. K., Hanson, D. A. & Schlaepfer, D. D. Focal adhesion kinase: in command and control of cell motility. Nat. Rev. Mol. Cell Biol. 6, 56–68 (2005).

34. Wehrle-Haller, B. Structure and function of focal adhesions. Curr. Opin. Cell Biol. 24, 116–124 (2012).

35. Loeser, R. F. Integrins and chondrocyte-matrix interactions in articular cartilage. Matrix Biol. 39, 11–16 (2014).

36. Manning, B. D. & Toker, A. AKT/PKB signaling: navigating the network. Cell 169, 381–405 (2017).

37. Wilusz, R. E., Sanchez-Adams, J. & Guilak, F. The structure and function of the pericellular matrix of articular cartilage. Matrix Biol. 39, 25–32 (2014).

Acknowledgements

We thank the reviewers for their comments.We thank all participants and staff involved in this study.This research was supported by the 910th Hospital of PLA Development Specialized programs.

Funding

This research was supported by the Science and Technology Planning Project of Quanzhou City, Fujian Province (No. 2025QZN05).

Author contributions

Longquan Lin, Huimin Cai, Peiji Chen contributed equally to this work and are co-first authors. Longquan Lin, Ruijin You and Peiji Chen are co-corresponding authors. Conceptualization: L.L., P.C. and H.C.; Methodology: L.L., P.C. and H.C.; Software: R.C., L.L. and H.C.; Formal analysis: K.C. and H.C.; Investigation: P.C. and H.C.; Resources: G.C. and D.L.; Data curation: H.C. and K.C.; Writing—original draft: L.L., P.C. and H.C.; Writing—review & editing: P.C.; Visualization: H.C.; Supervision: R.Y.; Project administration: R.Y.; Funding acquisition: L.L. and R.Y.All authors have read and agreed to the published version of the manuscript.

Competing interests

The authors declare no competing interests.

Ethics declarations

Approval for human experiments

The study was conducted in accordance with the Declaration of Helsinki and approved by the Ethics Committee of the 910th Hospital of PLA (Approval No. [2024]94). Informed consent was obtained from all subjects involved in the study.

Approval for animal experiments

The animal study was reviewed and approved by the Animal Ethics Committee of the 910th Hospital of PLA (Approval No. [2025]19). All animal experiments were conducted in accordance with the ARRIVE guidelines and the National Institutes of Health Guide for the Care and Use of Laboratory Animals.

Figure legends

Figure 1. Establishment of the mouse intervertebral disc degeneration (IVDD) model. (a) Surgical procedure of the needle-puncture model: anesthesia and positioning,dorsal incision to expose the disc, puncture of the disc through the annulus fibrosus, and suturing after surgery. (b) Gross morphology of representative discs: control group and model group.

Figure 2. Bioinformatics identification of ECM metabolism-related DEGs and the core hub gene COL6A2 in IVDD. (a) Volcano plot of DEGs in GSE70362 (IVDD_S vs. IVDD_M, n = 48; $|logFC| > 0.55$, $P < 0.05$). (b) Volcano plot of DEGs in GSE124272 (IVDD vs. healthy). Red, upregulated; blue, downregulated; gray, not significant. (c) Venn diagram showing the intersection of DEGs from GSE70362 and GSE124272 with ECM-related genes from PathCards. A total of 39 genes were shared, including COL6A2, LAMC1, ITGA9, ACAN (Aggrecan), MMP1, and MMP2. (d) Functional enrichment of the 39 ECM-related DEGs: top 10 GO biological processes and KEGG pathway enrichment. Bubble size indicates the number of genes; color indicates significance (-log10 P). (e) PPI network and KEGG pathway correspondence. Square nodes are KEGG pathways; circular nodes are genes; node size reflects connectivity. COL6A2 had the highest MCC score (4,004,950) and was the core hub gene, followed by COL5A2 (4,004,664) and COL12A1 (4,004,522).

Figure 3. Histopathology of the degenerated disc. Disc sections from control (I1, n = 3) and model (J1, n = 8) mice were stained with HE, Safranin O/fast green, and toluidine blue. Scale bar, 200 μm. The control group showed intact intervertebral disc structure, normal histomorphology of the nucleus pulposus (NP) tissue, and a rich ECM; the model group showed damage to the intervertebral discs, reduced proteoglycan content (Safranin O staining), and diminished staining of the cartilage.

Figure 4. Validation of COL6A2 knockdown and its effect on ECM-related gene expression in NP cells. (a) RT-qPCR screening of COL6A2 mRNA levels in NP cells transduced with three independent COL6A2-targeting shRNAs (COL6A2 shRNA-1, COL6A2 shRNA-2 and COL6A2 shRNA-3); the control and shRNA-NC groups served as negative controls, and COL6A2 shRNA-1 exhibited the highest knockdown efficiency (about 73.6%). (b–e) RT-qPCR detection of ECM-related genes (b) ADAMTS-8, (c) Aggrecan, (d) LAMC1, and (e) ITGA9 in NP cells transduced

with control, shRNA-NC or COL6A2 shRNA-1 lentiviruses. COL6A2 silencing reduced all four genes (ADAMTS-8, $P < 0.0001$; Aggrecan, $P = 0.0006$; LAMC1, $P = 0.0011$; ITGA9, $P < 0.0001$). Data are means ± SD. **$P < 0.01$, ***$P < 0.001$ vs. control; ##$P < 0.01$, ###$P < 0.001$ vs. shRNA-NC. ns, not significant.

Figure 5. COL6A2 knockdown reduces ECM-related protein expression in NP cells. (a) Representative Western blots of ADAMTS-8, Aggrecan, and beta-actin in the control, shRNA-NC, and COL6A2 shRNA-1 groups. Three independent experiments gave similar results. (b, c) Densitometric analysis of (b) ADAMTS-8 and (c) Aggrecan normalized to beta-actin. ADAMTS-8 fell from 0.51 ± 0.10 (control) to 0.16 ± 0.08 (COL6A2 shRNA-1; $P = 0.0037$); Aggrecan fell from 0.82 ± 0.12 to 0.17 ± 0.09 ($P = 0.0003$). Data are means ± SD with individual points. **$P < 0.01$, ***$P < 0.001$.

Figure 6. COL6A2 knockdown impairs NP cell migration and proliferation. (a) Wound healing assay: bright-field images of scratches at 0, 12, and 24 h (scale bar, 200 μm) and wound closure rates; (b) the COL6A2 shRNA-1 group migrated less at both time points (12 h: 19.5% ± 1.2% vs. 29.1% ± 0.9%, $P < 0.001$; 24 h: 48.7% ± 1.2% vs. 77.7% ± 0.7%, $P < 0.0001$). (c) CCK-8 assay of relative proliferation: 100.0% ± 7.0% (control), 96.9% ± 4.9% (shRNA-NC; $P = 0.387$ vs. control), and 54.3% ± 8.4% (COL6A2 shRNA-1; $P < 0.0001$ vs. control). Data are means ± SD ($n = 6$) with individual points. **$P < 0.01$, ***$P < 0.001$.

Figure 7. Depletion of COL6A2 restrains phosphorylation-mediated activation of the FAK/PI3K-Akt/ERK cascade in NP cells. (a) Representative Western blot profiles showing p-PI3K, PI3K, p-FAK, FAK, p-Akt, Akt, p-ERK1/2, ERK1/2, and β-actin in NP cells from the shRNA-NC and COL6A2 shRNA-1 groups. (b) Densitometric quantification of phosphorylated proteins relative to their corresponding total proteins. COL6A2 knockdown led to a marked reduction in p-PI3K, p-FAK, p-Akt, and p-ERK1/2 levels, whereas total protein expression remained largely unaltered. Data are presented as mean ± SD (n=3). *$P<0.05$, **$P<0.01$.

Figure 8. Pharmacologic blockade of PI3K-Akt phenocopies the ECM profile induced by COL6A2 silencing. (a) CCK-8 assay assessing relative proliferation of NP cells treated with LY294002 (10, 15, 20 μM) for 48 h, identifying 15 μM as the maximal non-cytotoxic dose. (b) Representative immunoblots of p-Akt, Akt, ADAMTS-8, Aggrecan, and β-actin in DMSO- and LY294002 (15 μM)-treated NP cells. (c) Densitometric analysis: LY294002 curtailed p-Akt, ADAMTS-8, and Aggrecan expression without altering t-Akt. Data are mean ± SD (n=3). *$P<0.05$, **$P<0.01$.

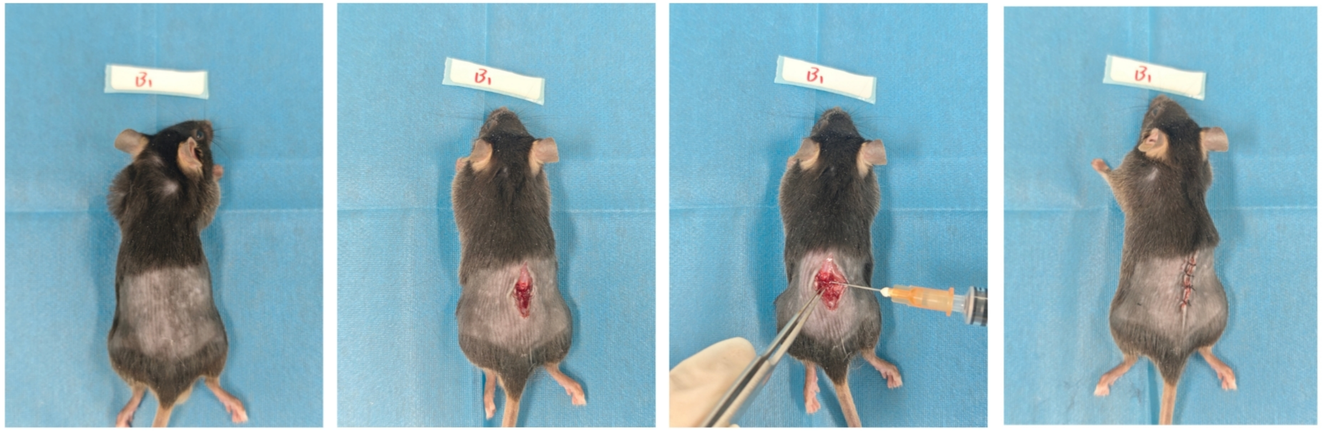
Tables

Table 1. Primer sequences used in this study

Gene	Accession No.	Direction	Primer sequence (5′–3′)	Tm (℃)	CG %	Product size (bp)
M-ACTIN	NM_007393.5	sense	CTGAGAGGGAAATCGTGCGT	60	55	208
		antisense	CCACAGGATTCCATACCCAAGA	61.3	50	

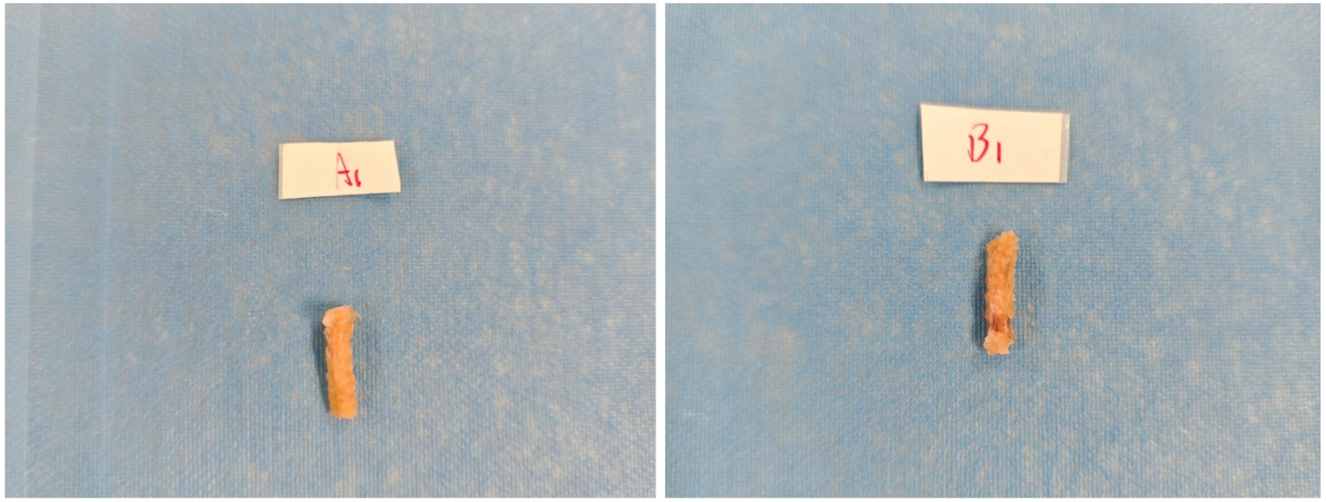
M-COL6A2	NM_146007	sense	AGAGCTCTATGTGGCCCAGT	60.3	55	242
		antisense	TGGTGGTCACGTTGTAGGTC	59.6	55	
M-LAMC1	NM_010683	sense	ACATGCCAGCGAGTGTGTAA	59.9	50	161
		antisense	AGTCACAAGGAAGGCACTCG	59.9	55	
M-ITGA9	NM_133721	sense	TACAACCTGGACGCGCA	58.9	58.8	191
		antisense	GGGTTGGTATGGACACGACA	59.7	55	
M-ADAMTS-8	NM_013906	sense	GGCAACGGCGTTTCAACAAG	60.0	55	223
		antisense	CTGAGAACGTGCCCTAGCTC	59.8	60	
M-Aggrecan	NM_007424	sense	CCTGCTACTTCATCGACCCC	59.8	60	150
		antisense	AGATGCTGTTGACTCGAACCT	60.6	47.6	
H-COL6A2	NM_001849	sense	AGCCTACGGAGAGTGCTACA	60.0	55	173
		antisense	GTCCTGGGAATCCAATGGGG	59.8	60	

a

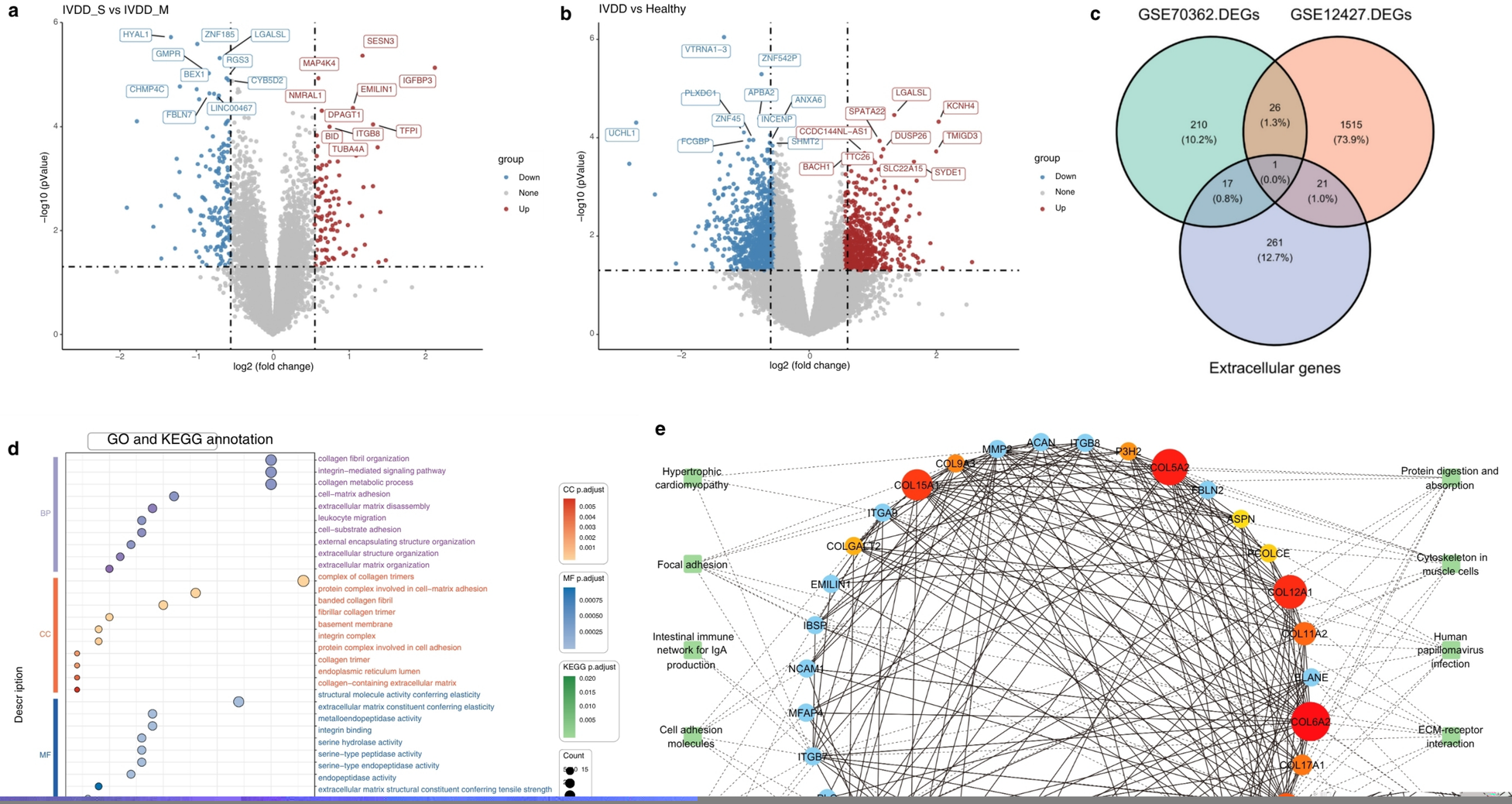


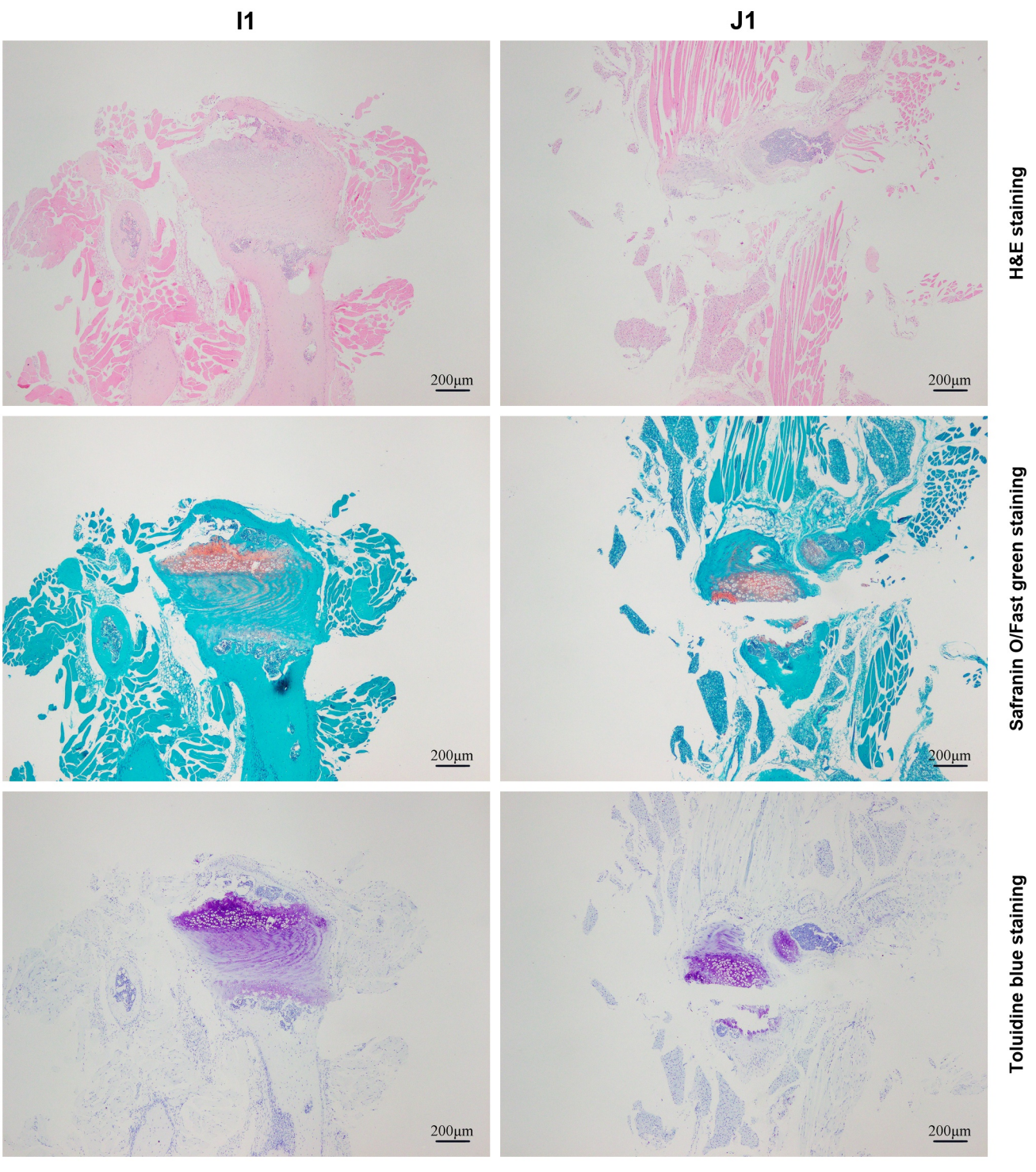
Anesthesia | Surgical Exposure | Needle Puncture | Post-operative

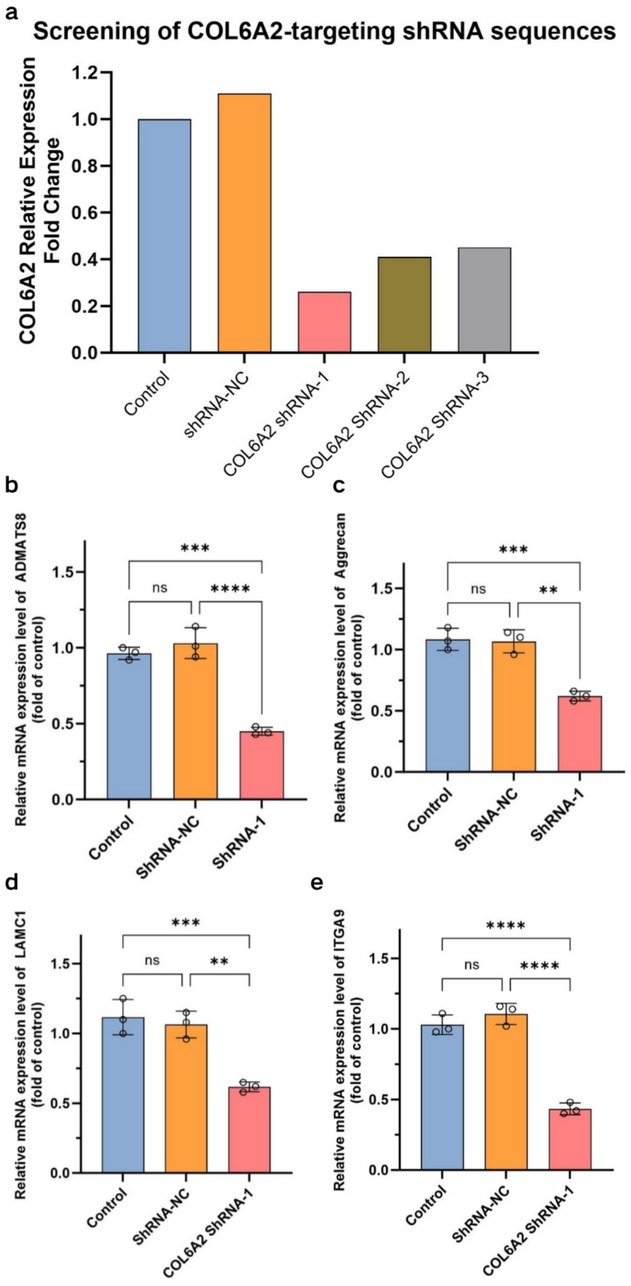
b

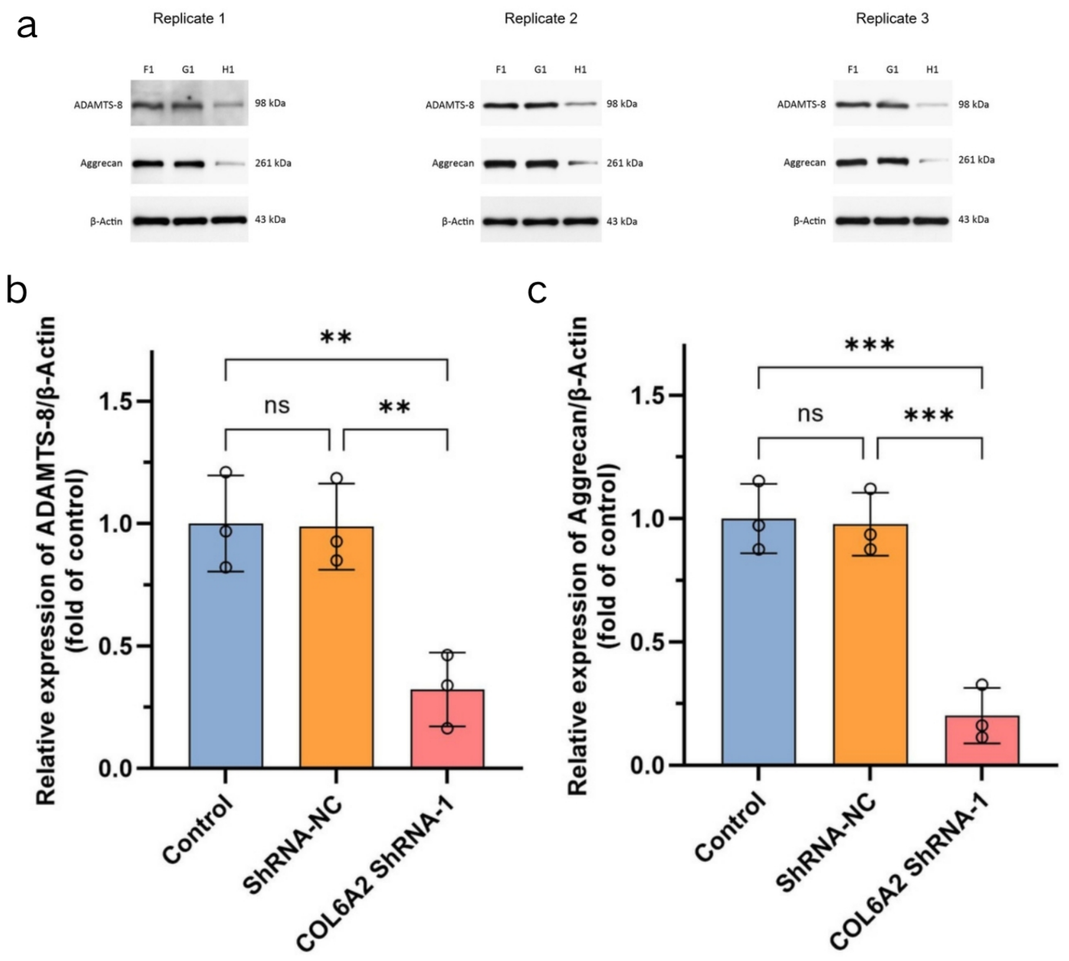


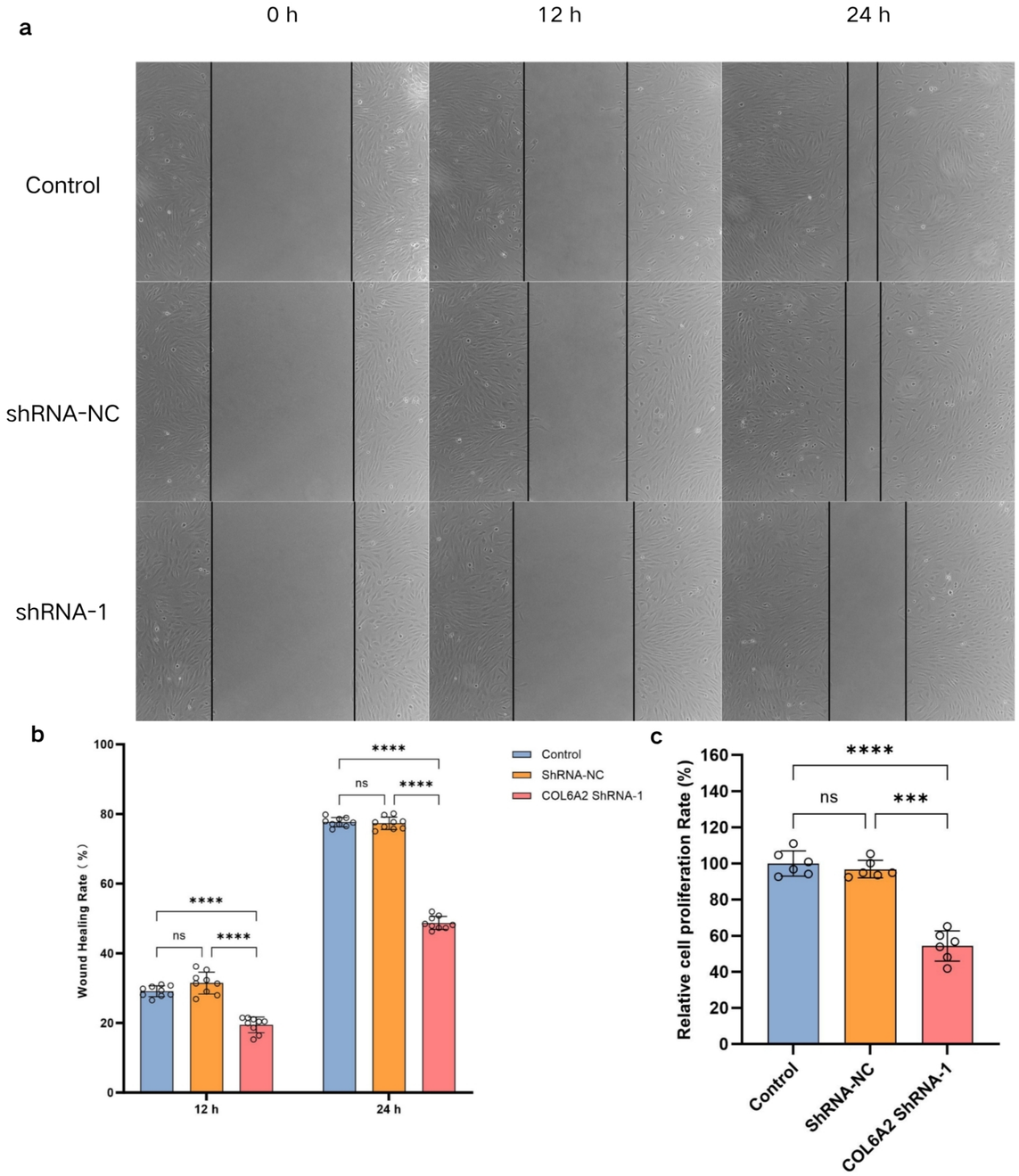
Control | Model

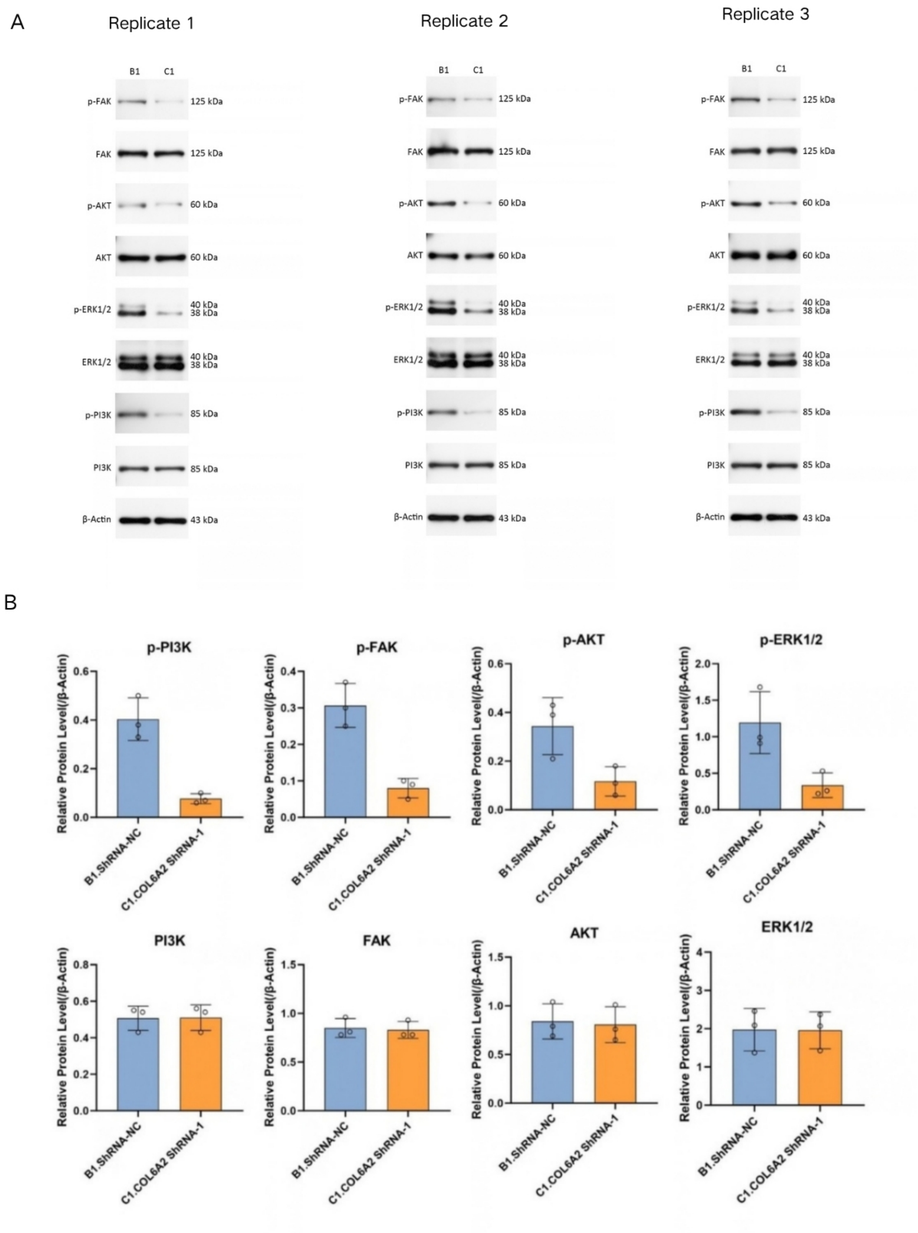

a
IVDD_S vs IVDD_M
HYAL1
ZNF185
LGALSL
GMPR
RGS3
SESN3
MAP4K4
BEX1
CYB5D2
IGFBP3
CHMP4C
NMRAL1
EMILIN1
LINC00467
FBLN7
DPAGT1
TFPI
BID
ITGB8
TUBA4A
−log10 (pValue)
log2 (fold change)
group
Down
None
Up
b
IVDD vs Healthy
VTRNA1−3
ZNF542P
PLXDC1
APBA2
ANXA6
LGALSL
KCNH4
ZNF45
INCENP
SPATA22
UCHL1
CCDC144NL−AS1
DUSP26
TMIGD3
FCGBP
SHMT2
BACH1
TTC26
SLC22A15
SYDE1
−log10 (pValue)
log2 (fold change)
group
Down
None
Up
c
GSE70362.DEGs
GSE12427.DEGs
210
(10.2%)
26
(1.3%)
1515
(73.9%)
1
(0.0%)
17
(0.8%)
21
(1.0%)
261
(12.7%)
Extracellular genes
d
GO and KEGG annotation
BP
CC
MF
Descr iption
collagen fibril organization
integrin−mediated signaling pathway
collagen metabolic process
cell−matrix adhesion
extracellular matrix disassembly
leukocyte migration
cell−substrate adhesion
external encapsulating structure organization
extracellular structure organization
extracellular matrix organization
complex of collagen trimers
protein complex involved in cell−matrix adhesion
banded collagen fibril
fibrillar collagen trimer
basement membrane
integrin complex
protein complex involved in cell adhesion
collagen trimer
endoplasmic reticulum lumen
collagen−containing extracellular matrix
structural molecule activity conferring elasticity
extracellular matrix constituent conferring elasticity
metalloendopeptidase activity
integrin binding
serine hydrolase activity
serine−type peptidase activity
serine−type endopeptidase activity
endopeptidase activity
extracellular matrix structural constituent conferring tensile strength
CC p.adjust
0.005
0.004
0.003
0.002
0.001
MF p.adjust
0.00075
0.00050
0.00025
KEGG p.adjust
0.020
0.015
0.010
0.005
Count
e
Hypertrophic cardiomyopathy
Focal adhesion
Intestinal immune network for IgA production
Cell adhesion molecules
Protein digestion and absorption
Cytoskeleton in muscle cells
Human papillomavirus infection
ECM-receptor interaction
MMP2
ACAN
ITGB8
P3H2
COL9A3
COL5A2
COL15A1
FBLN2
ITGA8
ASPN
COLGALT2
PCOLCE
EMILIN1
COL12A1
IBSP
COL11A2
NCAM1
FLANE
MFAP4
COL6A2
ITGB5
COL17A1

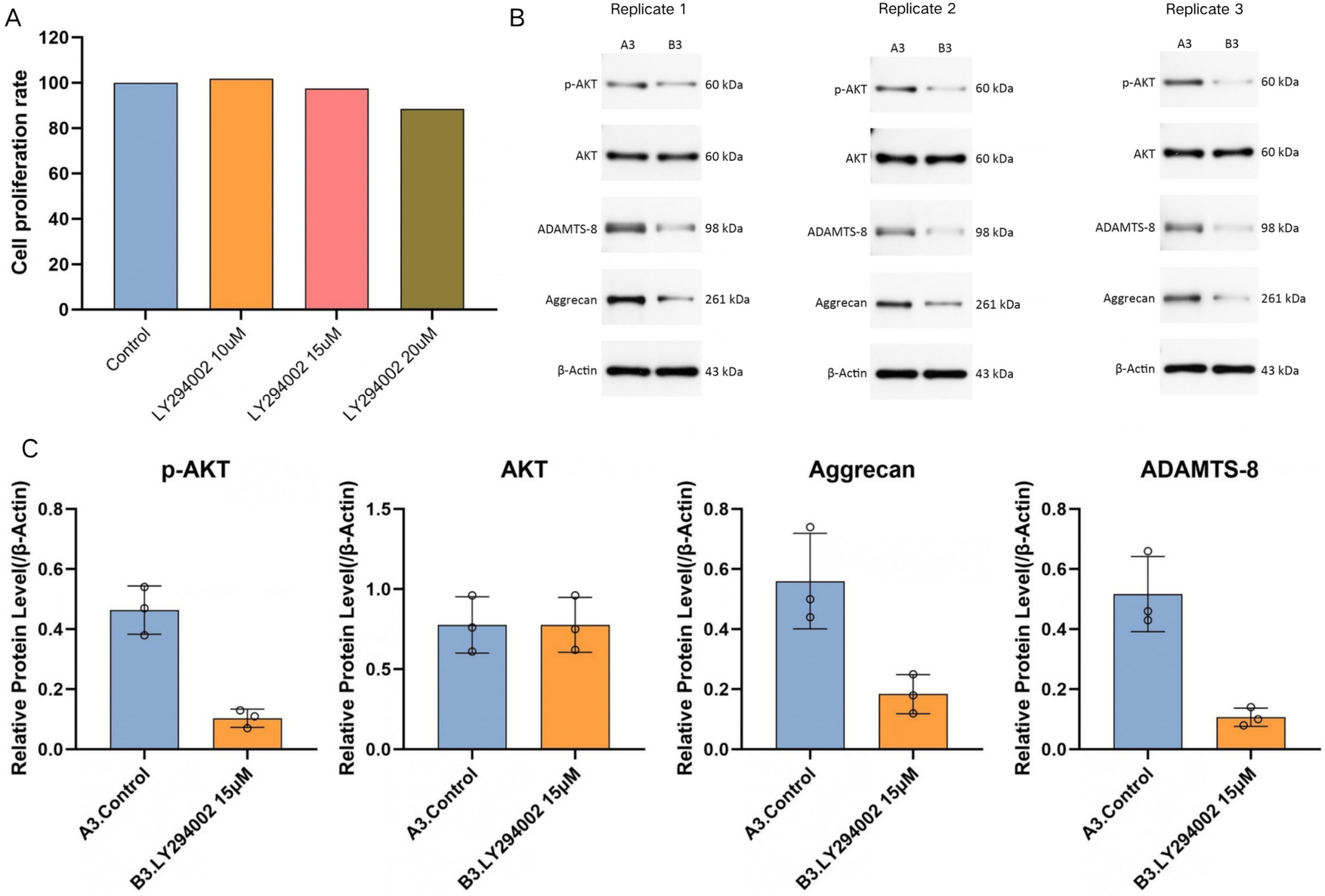

I1
J1
H&E staining
Safranin O/Fast green staining
Toluidine blue staining
200μm
200μm
200μm
200μm
200μm
200μm


a
Screening of COL6A2-targeting shRNA sequences
COL6A2 Relative Expression Fold Change
1.2
1.0
0.8
0.6
0.4
0.2
0.0
Control
shRNA-NC
COL6A2 shRNA-1
COL6A2 ShRNA-2
COL6A2 ShRNA-3
b
Relative mRNA expression level of ADMATS8 (fold of control)
***
ns
****
1.5
1.0
0.5
0.0
Control
ShRNA-NC
ShRNA-1
c
Relative mRNA expression level of Aggrecan (fold of control)
***
ns
**
1.5
1.0
0.5
0.0
Control
ShRNA-NC
ShRNA-1
d
Relative mRNA expression level of LAMC1 (fold of control)
***
ns
**
1.5
1.0
0.5
0.0
Control
ShRNA-NC
COL6A2 ShRNA-1
e
Relative mRNA expression level of ITGA9 (fold of control)
****
ns
****
1.5
1.0
0.5
0.0
Control
ShRNA-NC
COL6A2 ShRNA-1


a
Replicate 1
Replicate 2
Replicate 3
F1
G1
H1
ADAMTS-8
98 kDa
Aggrecan
261 kDa
β-Actin
43 kDa
b
Relative expression of ADAMTS-8/β-Actin (fold of control)
**
ns
**
1.5
1.0
0.5
0.0
Control
ShRNA-NC
COL6A2 ShRNA-1
c
Relative expression of Aggrecan/β-Actin (fold of control)
***
ns
***
1.5
1.0
0.5
0.0
Control
ShRNA-NC
COL6A2 ShRNA-1


a
0 h
12 h
24 h
Control
shRNA-NC
shRNA-1
b
Wound Healing Rate（%）
100
80
60
40
20
0
****
ns
****
****
ns
****
12 h
24 h
Control
ShRNA-NC
COL6A2 ShRNA-1
c
Relative cell proliferation Rate (%)
160
140
120
100
80
60
40
20
0
****
ns
***
Control
ShRNA-NC
COL6A2 ShRNA-1


A
Replicate 1
Replicate 2
Replicate 3
B1
C1
p-FAK
FAK
p-AKT
AKT
p-ERK1/2
ERK1/2
p-PI3K
PI3K
β-Actin
125 kDa
60 kDa
40 kDa
38 kDa
85 kDa
43 kDa
B
p-PI3K
p-FAK
p-AKT
p-ERK1/2
PI3K
FAK
AKT
ERK1/2
Relative Protein Level(/β-Actin)
B1.ShRNA-NC
C1.COL6A2 ShRNA-1


A
Cell proliferation rate
120
100
80
60
40
20
0
Control
LY294002 10uM
LY294002 15uM
LY294002 20uM
B
Replicate 1
Replicate 2
Replicate 3
A3
B3
p-AKT
AKT
ADAMTS-8
Aggrecan
β-Actin
60 kDa
98 kDa
261 kDa
43 kDa
C
p-AKT
AKT
Aggrecan
ADAMTS-8
Relative Protein Level(/β-Actin)
A3.Control
B3.LY294002 15μM

Supplementary Files

This is a list of supplementary files associated with this preprint. Click to download.

- PharmacologicalinhibitionofthePI3KAktpathwayWB0222.pdf
- PharmacologicalinhibitionofthePI3KAktpathwayWB0212.pdf
- PharmacologicalinhibitionofthePI3KAktpathwayWB0232.pdf
- ExpressionofECMrelatedproteinsafterknockdownofCOL6A2WB032.pdf
- ExpressionofECMrelatedproteinsafterknockdownofCOL6A2WB022.pdf
- DetectionofphosphorylationpathwaysafterCOL6A2knockdownWB0122.pdf
- DetectionofphosphorylationpathwaysafterCOL6A2knockdownWB0132.pdf
- ExpressionofECMrelatedproteinsafterknockdownofCOL6A2WB012.pdf
- DetectionofphosphorylationpathwaysafterCOL6A2knockdownWB0112.pdf